PHYSICAL REVIEW B **92**, 224408 (2015)

Magnetic structure of the quasi-two-dimensional antiferromagnet $NiPS_3$

A. R. Wildes,[1,*] V. Simonet,[2,3] E. Ressouche,[4] G. J. McIntyre,[5] M. Avdeev,[5] E. Suard,[1] S. A. J. Kimber,[6] D. Lançon,[1,7] G. Pepe,[8,†] B. Moubaraki,[9] and T. J. Hicks[10]

[1]*Institut Laue-Langevin, CS 20156, 38042 Grenoble Cédex 9, France*

[2]*CNRS, Institut Néel, F-38000 Grenoble, France*

[3]*Univ. Grenoble Alpes, Institut Néel, F-38000 Grenoble, France*

[4]*CEA-Grenoble/INAC, Laboratoire MDN, 17 rue des martyrs, 38054 Grenoble Cédex 9, France*

[5]*Australian Nuclear Science and Technology Organisation, Locked Bag 2001, Kirrawee DC NSW 2232, Australia*

[6]*European Synchrotron Radiation Facility, CS40220, 38043 Grenoble Cédex 9, France*

[7]*Ecole Polytechnique Fédérale de Lausanne, SB ICMP LQM, CH-1015 Lausanne, Switzerland*

[8]*Department of Physics and Astronomy, University College London, Gower Street, London WC1E 6BT, United Kingdom*

[9]*School of Chemistry, Monash University, Box 23, Clayton, Vic 3800, Australia*

[10]*School of Physics, Monash University, Box 27, Clayton, Vic 3800, Australia*

(Received 15 June 2015; revised manuscript received 6 November 2015; published 7 December 2015)

The magnetic structure of the quasi-two-dimensional antiferromagnet $NiPS_3$ has been determined by magnetometry and a variety of neutron diffraction techniques. The experiments show that the samples must be carefully handled, as gluing influences the magnetometry measurements while preferred orientation complicates the interpretation of powder diffraction measurements. Our global set of consistent measurements show numerous departures from previously published results. We show that the compound adopts a $\mathbf{k} = [010]$ antiferromagnetic structure with the moment directions mostly along the a axis, and that the paramagnetic susceptibility is isotropic. The critical behavior was also investigated through the temperature dependence of the magnetic Bragg peaks below the Néel temperature.

DOI: 10.1103/PhysRevB.92.224408 PACS number(s): 75.25.−j, 75.50.Ee, 75.40.Cx

I. INTRODUCTION

The MPS_3 (M = Mn, Fe, Co, Ni) family of compounds are quasi-two-dimensional materials [1]. Their structures have similarities to graphite. The transition metal atoms lie on a honeycomb lattice in the ab planes, which are weakly bound by van der Waals forces. The transition metal atoms have a 2+ electronic ionization state and thus carry a localized magnetic moment. All of the compounds adopt an ordered antiferromagnetic structure at low temperature [2]. The compounds are rare examples of materials with two-dimensional characteristics in both the atomic and magnetic structures.

The compounds have numerous properties that make them interesting for application in batteries and optoelectronics, including the ability to be intercalated [1]. As a result, research on these compounds has mostly focused on their chemical and electronic properties. In comparison, the magnetic properties have been largely overlooked. This is despite the fact that they are rare examples of model magnetic systems on a two-dimensional honeycomb lattice, and that changing the metal ion causes the magnetic properties to be very different. For example, $MnPS_3$ largely behaves like a Heisenberg antiferromagnet, while $FePS_3$ has the properties of an Ising antiferromagnet [3]. Closer examination shows small, but important, departures from ideal behavior: $MnPS_3$ displays magnetoelectric behavior [4] and has a small X-Y anisotropy that dominates the critical behavior of the magnetism [5]; the spin dynamics of $FePS_3$ are best described using a Heisenberg Hamiltonian with a large anisotropy and they show that the compound may be close to being a one-dimensional ferromagnet [6]. These compounds may thus provide a fertile test bed for theories of magnetism and anisotropy in low dimensions.

The crystallographic structures for the family all have monoclinic symmetry with space group $C2/m$, and the atomic positions have been precisely determined by x-ray diffraction on single crystals [7]. Neutron powder diffraction was used to investigate the magnetic structures for all the members of the family during the 1970s and 1980s and the findings are summarized in a review by Brec [2]. However, recent experiments on single crystals of some of the compounds have shown the previously published magnetic structures to be somewhat in error. $MnPS_3$ was said to have a magnetic propagation vector of $\mathbf{k} = 0$, with each Mn^{2+} ion being antiferromagnetically coupled to its three nearest neighbors and with its moment pointing normal to the ab planes. Single crystal neutron diffraction showed that the structure is indeed $\mathbf{k} = 0$, but that the moments pointed $\sim 8^\circ$ from the c^* axis [4]. A bigger difference was found in $FePS_3$. The originally published structure had a propagation vector of $\mathbf{k} = [01\frac{1}{2}]$, while a more recent study showed that the propagation vector is $\mathbf{k} = [\frac{1}{2}\frac{1}{2}0.34]$ [8]. The iron moments are collinear with the normal to the ab planes in both structures.

An explanation for the discrepancies could be due to the difficulties in dealing with preferred orientation in powder diffraction experiments on these samples. The compounds take the form of very soft platelets. Crystals are not easily crushed when attempting to grind them to a powder. Instead, the ab planes, being weakly bound by van der Waals forces, tend to slide across one another when a shear force is applied. It is consequently very difficult to create isotropic powders,

*wildes@ill.fr

†Present address: Department of Physics, Cavendish Laboratory, 19 J. J. Thomson Avenue, Cambridge CB3 0HE, United Kingdom.

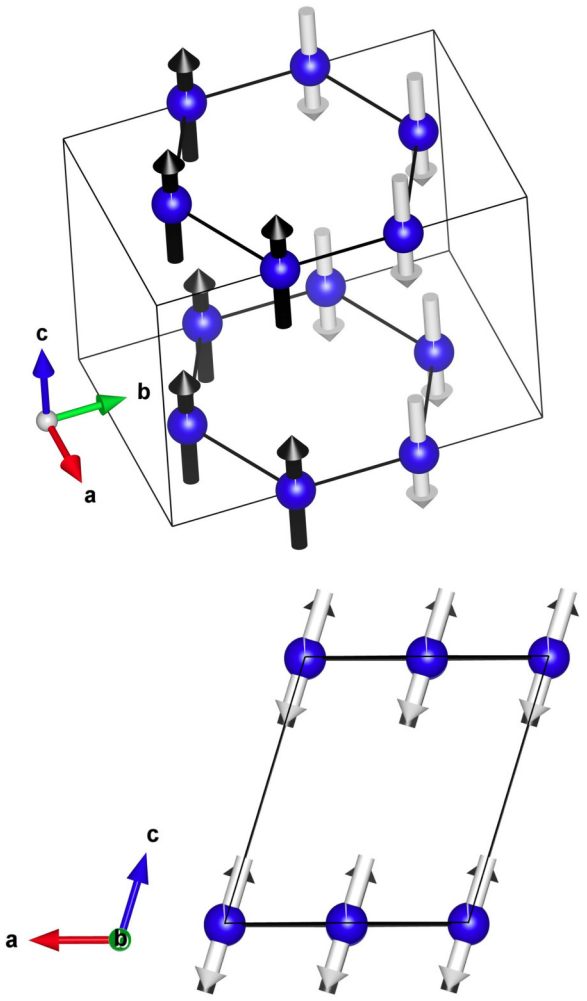

FIG. 1. (Color online) A schematic of the published magnetic structure of $NiPS_3$ [2]. The moments are on the Ni sites. The figure was created using the VESTA program [13].

and samples tend to show substantial texture and preferred orientation.

$NiPS_3$ is another member of the MPS_3 family and may also be an example of a model magnetic system. Magnetic susceptibility measurements on single crystals [3,9] showed the Ni^{2+} ions to have spin $S = 1$ and fits to the high-temperature susceptibility gave effective moments that were very close to the spin-only values [3]. The paramagnetic susceptibilities also showed the compound to be anisotropic, leading the authors to conclude that a combination of lattice distortion and spin-orbit coupling caused $NiPS_3$ to be best described by an anisotropic Heisenberg Hamiltonian.

The susceptibilities below the Néel temperature of $T_N = 155$ K suggested that the moments lie in the ab planes [3,9]. This conclusion is not consistent with the magnetic structure of $NiPS_3$ that was determined from neutron powder diffraction and is shown schematically in Fig. 1. The antiferromagnetic structure is quoted to have a $\mathbf{k} = [010]$ propagation vector with the moments pointing along the c axis [2].

Besides being a potential candidate for a model magnetic system, $NiPS_3$ has added interest as it has similarities with some compounds that are currently highly investigated. The $\mathbf{k} = [010]$ antiferromagnetic structure on a honeycomb lattice is identical to the "zigzag" magnetic order observed in Na_2IrO_3, a candidate for a system driven by a Kitaev-Heisenberg spin Hamiltonian [10]. $NiPS_3$ also shows evidence for two-magnon excitations in Raman scattering which gives it similarities with cuprate superconductors [11,12]. It is therefore of interest to know the magnetic structure of this compound to understand the symmetry of the magnetic Hamiltonian and thus to derive the dynamics. The discrepancies discovered with the magnetic structures of $MnPS_3$ and $FePS_3$, and the contradictory results of neutron diffraction and magnetization measurements for $NiPS_3$, show that it is timely to reexamine the magnetic structure of $NiPS_3$.

In this article we report the results from a study of the magnetization and magnetic structure of $NiPS_3$ using SQUID magnetometry, x-ray powder diffraction, and neutron diffraction on both powders and single crystals. We present our best results, leading to an updated magnetic structure for $NiPS_3$ that is consistent between magnetization and diffraction measurements. Our results show many discrepancies with previously published results. The discrepancies may be attributed to two effects that have a major impact on the data and its interpretation: the inability to analyze correctly powder diffraction data due to the presence of preferred orientation; and the distortion of magnetization data when a crystal is glued to its support. The influence of these effects are described in the Supplemental Material [14]. We also present data showing the critical behavior of the sublattice magnetization for $T < T_N$.

II. EXPERIMENTS

A. Sample preparation

Crystal samples of $NiPS_3$were grown by a vapor transport method, following previously published protocols [1,2]. Quartz tubes were cleaned internally by etching with acid, then rinsed with demineralized water and finally heated, under vacuum, to 1000 °C for 30 min. Stoichiometric quantities of nickel, phosphorus, and sulfur of purity 99.998% or better were placed into the tube under an argon atmosphere. The total mass of the ingredients in a tube was 5 g. The tubes were then evacuated, sealed under vacuum, and placed in a two-zone horizontal furnace. One end of the quartz tube, containing the ingredients, was positioned in zone 1 of the furnace while the other end was positioned in zone 2. The two zones of the furnace were then independently heated and maintained at temperature for a period of time following the two-stage protocol listed in Table I. The two zones were then simultaneously switched off and allowed to cool.

A resulting tube contained a large number of platelet crystals with the characteristic hexagonal motif and metallic gray color of $NiPS_3$. A few platelets of what appeared to be the best examples of single crystals were put aside. They

TABLE I. Table showing the set temperatures and durations of the two-zone growth furnace used for the synthesis of $NiPS_3$.

Stage	Zone 1 (°C)	Zone 2 (°C)	Duration (days)
1	700	750	2
2	670	620	16

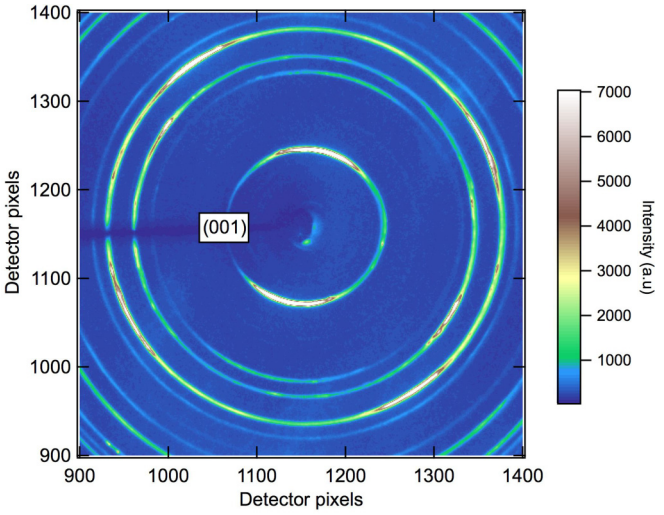

FIG. 2. (Color online) Raw detector image for high energy x-ray powder diffraction from $NiPS_3$. The data show strong texture due to preferred orientation. The (001) diffraction ring is highlighted, which shows a particularly pronounced intensity variation with azimuthal angle.

had typical dimensions of $\sim 3 \times 2 \times 0.5$ mm^3 and a mass of $\sim$10 mg. The rest were ground into powder.

B. High-energy x-ray powder diffraction

The ID15B diffractometer at the European Synchrotron Radiation Facility (ESRF), France, was used to characterize the crystal structure of the samples using transmission high-energy powder diffraction. A small quantity of powdered sample was placed in a 2 mm Kapton tube, which did not move for the duration of the measurements. A wavelength of 0.1422 Å was used and the scattered x rays were detected by a Mar345 image plate. Energy calibration was performed by measuring a CeO_2 standard.

Strong preferred orientation, indicative of the difficulties in creating isotropic powders from these compounds, is apparent in the raw detector image in Fig. 2. However, the influence of preferred orientation is alleviated in the analysis of these data. The use of hard x rays and the two-dimensional detector meant that the intensity could be measured over the full Debye-Scherrer cone for a sufficient number of Bragg peaks for a quantitative Rietveld analysis [15] to be performed. The resulting powder diffraction pattern was more representative of an isotropic sample and was analyzed using the GSAS software suite [16].

The data and the results of the Rietveld analysis are shown in Fig. 3. The symmetry of the samples agreed with the expected $C2/m$ space group [17]. The calculated peak positions and intensities were in satisfactory agreement with the experimental data. Little adjustment to the cell parameters and internal degrees of freedom were required, proving that the influence of preferred orientation is minimized in the two-dimensional measuring geometry used here. Previous structural studies reported a small site disorder between the main $4g$ and the minority $2a$ sites for the Ni, and likewise for the main $4i$ and the minority $8j$ sites for the P [17]. This site disorder was permitted in the refinement. The stoichiometry

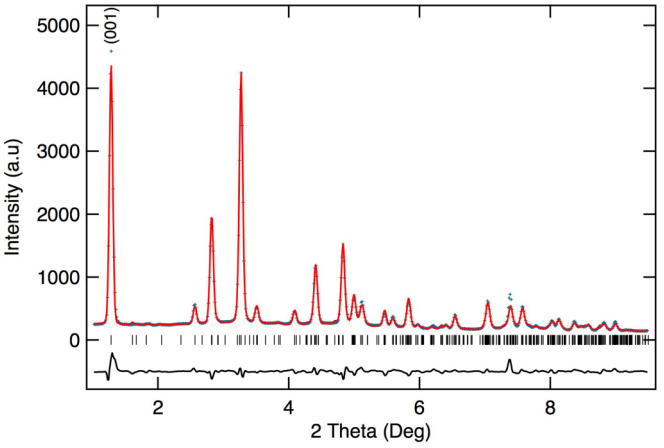

FIG. 3. (Color online) Observed (blue crosses), calculated (red line), and difference (black line) profiles from the Rietveld fit to the synchrotron x-ray diffraction pattern of $NiPS_3$.

was constrained to be $NiPS_3$, and the x and z coordinates for the P $4i$ and $8j$ positions were constrained to be equivalent. The site disorder is larger than previously estimated, however, it likely reflects stacking faults between the ab planes rather than an atomic site substitution. The refined values are given in Table II.

C. Magnetization measurements

Magnetometry measurements on single crystals were conducted using a MPMS SQUID magnetometer at the Institut Néel, Grenoble. Diffraction measurements were used to establish the high-symmetry directions in the crystal, which was then wrapped in plastic film and suspended within a plastic drinking straw. Measurements were taken with the field applied along three high symmetry directions, a, b, and c^*, the c^* axis being normal to the platelets and to the ab planes. The sample was removed from the magnetometer and realigned between measurements. Using this method to align the crystal was not overly precise, but was probably good to within $\pm 5^\circ$.

The magnetization (M) was measured as a function of temperature in applied fields of $H = 0.01$, 0.1, and 1 T. No substantial differences in M/H were observed between the measurements, nor were there differences between field-cooled and zero-field-cooled measurements. Magnetizations

TABLE II. Refined atomic coordinates for $NiPS_3$ at 295 K from synchrotron x-ray powder diffraction in space group $C2/m$. An occupancy of 1 indicates the Wyckoff position is fully occupied. The refined lattice parameters were $a = 5.840(1)$, $b = 10.141(2)$, $c = 6.651(1)$ Å, and $\beta = 107.13(3)^\circ$ and the residuals were ${}_wR_p = 6.55\%$ and $\chi^2 = 1.64$.

Atom	Wyckoff postion	x	y	z	Occupancy
Ni(1)	$4g$	0	0.328(2)	0	0.71(1)
P(1)	$4i$	0.063(5)	0	0.166(2)	0.71(1)
S(1)	$4i$	0.711(3)	0	0.240(2)	1
S(2)	$8j$	0.238(2)	0.174(2)	0.238(1)	1
Ni(2)	$2a$	0	0	0	0.58(2)
P(2)	$8j$	0.063(5)	0.380(5)	0.166(2)	0.15(6)

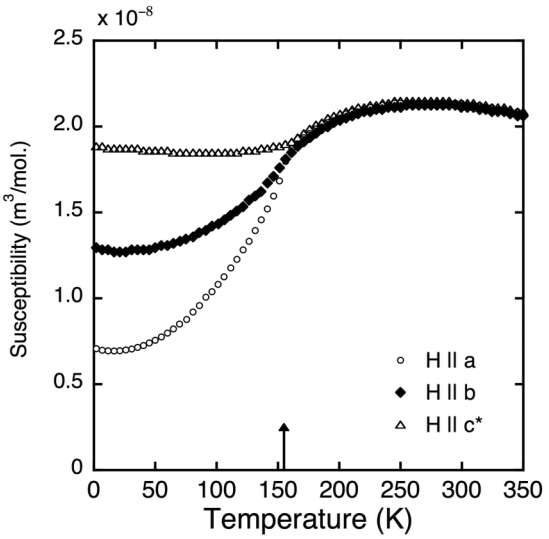

FIG. 4. Examples of the zero-field-cooled magnetic susceptibility of a $NiPS_3$ crystal measured along some high symmetry directions in an applied magnetic field of 0.1 T. No glue was used to mount the crystal. The arrow marks the expected Néel temperature of 155 K.

were also measured as a function of H at selected temperatures. Two samples were measured, and no substantial differences were observed between the data sets. An example of the temperature-dependent susceptibility, measured in an applied field of 0.1 T, is shown in Fig. 4, and the field-dependent magnetizations are shown in Fig. 5.

The data in Fig. 5 show that, up to the maximum field of 5 T, the magnetization increases linearly with applied field at all temperatures irrespective of the orientation with respect to the crystal. No evidence for extra phases or a spin flop transition was observed. The data in Fig. 4 show that the susceptibility (M/H) is isotropic above the Néel temperature of $T_N = 155$ K. There is a broad maximum above $T_N = 155$ K due to the two-dimensional nature of the magnetism, as seen

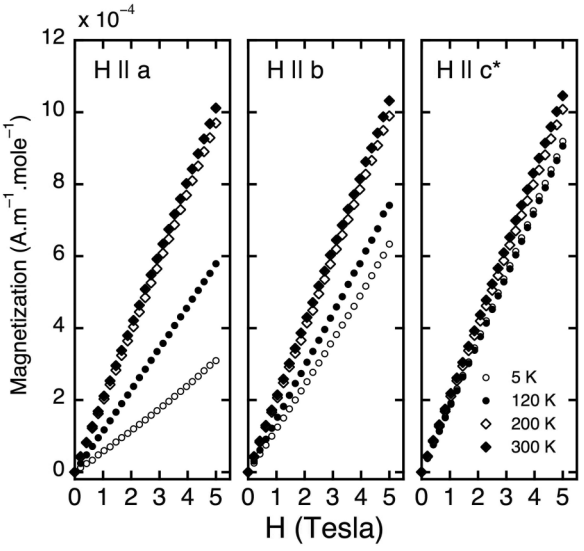

FIG. 5. The magnetization as a function of a field applied along some high symmetry directions of a $NiPS_3$ crystal at a selection of temperatures. No glue was used to mount the crystal.

in all the members of the MPS_3 family [3]. Below T_N, the susceptibility is largest and roughly constant when $H \parallel c^*$, showing that the moments lie mostly in the ab planes. The susceptibilities decrease as a function of temperature when the field is applied along a and b, with the former condition giving the steepest decrease. The ordered moments thus appear to point more towards the a axis than the b axis. Both conditions, however, plateau to nonzero susceptibilities at 0 K, meaning that in neither case was the field applied along a collinear moment direction. The maximum attainable temperature in the magnetometer was 350 K, which was not sufficiently high to observe Curie-Weiss behavior in the susceptibility.

The results in Fig. 4 show some consistencies with previously published data that showed the susceptibilities measured parallel and perpendicular to the c^* axis [3,9]. The Néel temperatures correspond between the data sets, as does the conclusion that the ordered moments lie in the ab planes. The previous results, however, showed that the susceptibility above T_N was anisotropic, with the parallel susceptibility ($H \parallel c^*$) being smaller than the perpendicular susceptibility ($H \perp c^*$). Our initial magnetization measurements were performed on samples that had been glued to their supports using shellac. As shown in the Supplemental Material [14], gluing the samples had a dramatic effect on the measurements, shifting the magnetization and resulting in data that could be wrongly attributed to anisotropic behavior. We assume that the use of glue has led to erroneous results in the previous studies [3,9,18].

A discussion of the possible interaction mechanisms between glue and $NiPS_3$ is beyond the scope of this article. However, it must be noted that these compounds may be intercalated with a variety of materials [1] and, being so soft, sample deformation on the thermal cycling of a glued sample is possible.

D. Unpolarized neutron powder diffraction

High resolution neutron powder diffraction experiments were carried out using the D2B diffractometer at the Institut Laue-Langevin. The instrument was configured to use 2.4 Å neutrons, and the diffraction was measured as a function of temperature using a helium cryostat. Due to reduced detector coverage and increased wavelength, D2B cannot measure a Bragg powder peak over a full Debye-Scherrer cone in the manner of ID15B and thus it was anticipated that preferred orientation would be an issue. A specific sample geometry was adopted in an attempt to overcome this. The powdered samples were separated into three parts of roughly equal mass. They were then pressed into cylindrical pellets of 10 mm diameter. The three pellets were then mounted such that their cylindrical axes were orthogonal before being lowered into the cryostat. The sample was then continuously rotated around the vertical axis as the diffraction patterns were collected.

Despite these efforts, the data were still highly influenced by preferred orientation. The best structure refinement using the FULLPROF suite [19] gave the expected $C2/m$ space group, lattice parameters, and atomic positions from the literature [17] and from Table II, however the quality of the fits were very poor. Attempts to account for the preferred orientation in the refinement showed that atomic positions and the preferred

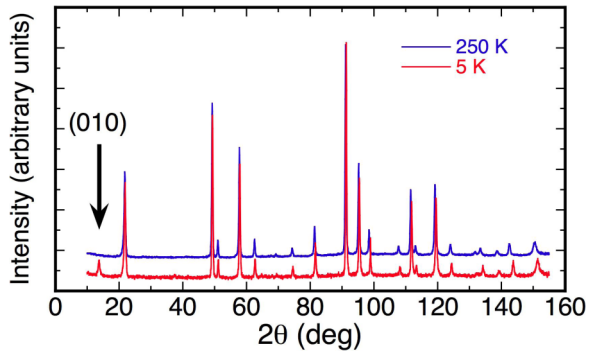

FIG. 6. (Color online) Neutron powder diffraction from $NiPS_3$, measured using a neutron wavelength of 2.4 Å, recorded above (250 K) and below (5 K) T_N. The data are shifted vertically for clarity. The only clear magnetic Bragg peak is at the (010) position, and it is marked on the figure.

orientation parameters were interdependent, and it was not possible to have full confidence in the fitted results. The data measured at 250 K, along with the best structure refinement before accounting for preferred orientation, are shown in the Supplemental Material [14].

However, a comparison of high and low temperature measurements was very revealing. The data at 250 and 5 K are superimposed in Fig. 6. Only one clear magnetic Bragg peak is visible in the 5 K data. It is found at the (010) position, which is systematically absent in the $C2/m$ space group, and is labeled in the figure. Subtraction plots of high- from low-temperature data did not show any other obvious peaks. As shown in the Supplemental Material [14], measurements with poorer resolution using the MRPD instrument at the Australian Nuclear Science and Technology Organization did not fare better.

The neutron powder diffraction data that were used to determine the magnetic structure in Fig. 1 were not published in a refereed journal [2], however it appears highly likely that these data also suffered from preferred orientation and from a paucity of magnetic Bragg peaks with sufficient intensity for an accurate structure determination. This may explain the discrepancy between the structure quoted from previous neutron measurements [2] and the structure concluded from magnetic susceptibility [3,9].

E. Polarized neutron powder diffraction

Neutron polarization analysis can separate nuclear from magnetic scattering and is thus a suitable technique to search for weak magnetic peaks in $NiPS_3$. Neutron powder diffraction measurements were performed using D7 at the Institut Laue-Langevin [20]. The instrument makes use of polarizing supermirrors in the incident and scattered beams to perform polarization analysis experiments. A neutron-spin flipper was positioned between the polarizer and the sample so that neutron non-spin-flip (NSF) and spin-flip (SF) scattering could be measured.

Measurements were performed on the same sample that was used for the D2B experiment, and in the same geometry within an aluminum holder. The neutron wavelength was 3.1 Å. The instrument was calibrated using an amorphous quartz sample for polarization efficiency, a vanadium sample for detector efficiency, and for normalization of the cross sections in absolute units. The background was estimated by measuring an empty sample holder with and without a cadmium insert. A liquid helium cryostat was used to control the temperature of the sample.

The neutron polarization direction at the sample was controlled using an electric-coil assembly, and the NSF and SF scattering were measured for three orthogonal polarization directions. In ideal conditions, these measurements allow three cross sections to be separated: the nuclear spin incoherent ($d\sigma_{\rm nsi}/d\Omega$); the magnetic ($d\sigma_{\rm mag}/d\Omega$); and a combination of the nuclear coherent ($d\sigma_{\rm coh}/d\Omega$) and isotopic incoherent ($d\sigma_{\rm ii}/d\Omega$) cross sections. The method is known as XYZ polarization analysis [20,21].

This analysis could successfully separate the cross sections at 300 K. Paramagnetic scattering with its characteristic form factor [22] was clearly visible in the magnetic cross section, and nuclear Bragg peaks compatible with the $C2/m$ space group were observed in $d\sigma_{\rm coh}/d\Omega$. A large nuclear spin-incoherent cross section, $d\sigma_{\rm nsi}/d\Omega = 1.866 \pm 0.002$ barn sr^{-1} (formula unit)$^{-1}$, was also discovered, most likely due to the presence of hydrogen which has a very large nuclear spin-incoherent cross section [23]. This may be due to some amorphization of the sample. Amorphous $NiPS_3$ is known to gain more than 10% of its weight in atmospheric water in less than one day [24,25], contrary to crystalline $NiPS_3$ which is not reported to be hydrophilic. Considering the softness of the samples, we assume that this amorphization occurs during the grinding process when preparing the powders. The level of amorphization may be estimated to be ≈15% from the $d\sigma_{\rm nsi}/d\Omega$ cross section and the 10% weight/weight ratio. The data at 300 K are shown in the Supplemental Material [14].

The XYZ method will only give a clean separation of the cross sections in the limit that the magnetic cross section depends on the magnitude, but not the direction, of $\mathbf{Q}$ [20]. This is true for paramagnets and isotropically powdered antiferromagnets, but proved not to be the case for $NiPS_3$ at low temperature, again due to the preferred orientation. The XYZ analysis of the data at 2 K resulted in substantial crosstalk between the magnetic and nuclear-spin incoherent signals. Consequently, only the data measured with the neutron polarization normal to the scattering plane were analyzed. In this configuration, the non-spin-flip ($d\sigma_{\rm NSF}/d\Omega$) and spin-flip ($d\sigma_{\rm SF}/d\Omega$) cross sections are given by the equations

$$\begin{aligned} \frac{d\sigma_{\rm NSF}}{d\Omega} &= \frac{d\sigma_{\rm coh}}{d\Omega} + \frac{d\sigma_{\rm ii}}{d\Omega} + \frac{1}{3}\frac{d\sigma_{\rm nsi}}{d\Omega} + \frac{d\sigma^{z}_{\rm mag}}{d\Omega}, \\ \frac{d\sigma_{\rm SF}}{d\Omega} &= \frac{2}{3}\frac{d\sigma_{\rm nsi}}{d\Omega} + \frac{d\sigma^{\perp}_{\rm mag}}{d\Omega}, \end{aligned} \tag{1}$$

where $d\sigma^{z}_{\rm mag}/d\Omega$ is the magnetic cross section due to those components of the sublattice magnetization that are normal to the scattering plane, and $d\sigma^{\perp}_{\rm mag}/d\Omega$ is from those components that are in the scattering plane and perpendicular to the scattering vector $\mathbf{Q}$.

The 2 K data are shown in Fig. 7. The $d\sigma_{\rm NSF}/d\Omega$ data show clear nuclear Bragg peaks that can be indexed with the $C2/m$ space group and their positions are marked with filled triangles.

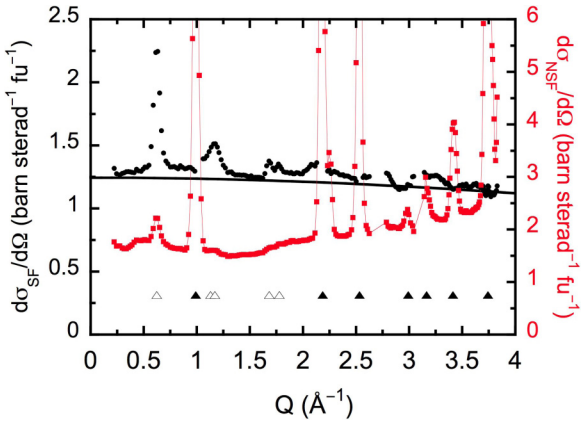

FIG. 7. (Color online) Spin-flip (black points) and non-spin-flip (red points) scattering from $NiPS_3$, measured with the polarization normal to the scattering plane. An estimation of 2/3 the nuclear spin incoherent scattering is shown as a solid black line. The positions of strong Bragg peaks for $NiPS_3$ calculated with $C2/m$ are shown as closed, black triangles. The positions of features in the spin-flip scattering, which must be magnetic, can be indexed in $P1$ and are shown as open triangles.

Substantial diffuse scattering, possibly due to nuclear short-ranged order from amorphous $NiPS_3$, is also visible, and the data also contain isotopic and nuclear-spin incoherent terms which are estimated to equal 1 barn sr^{-1} (formula unit)$^{-1}$. As for the D2B data, the peak at (010) is the only clear magnetic feature that is visible.

The spin-flip cross sections in Fig. 7 give the cleanest indication of the presence of additional magnetic Bragg peaks. The $d\sigma_{\rm nsi}/d\Omega$ contributions were estimated from the XYZ separation at 300 K, accounting for the change in the Debye-Waller factor between the two temperatures, and are also shown in the figure. The curve matches well to the minima in the measured $d\sigma_{\rm SF}/d\Omega$. The features above this incoherent contribution are due to magnetic scattering. A number of magnetic peaks are clearly visible at smaller Q. These peaks could be indexed with a $P1$ space group, which has the same symmetry as the $C2/m$ space group with a $\mathbf{k} = [010]$ magnetic structure. The expected positions for some $P1$ peaks are marked in the figure with open triangles, and they correspond to the positions of the magnetic Bragg peaks. The quality of the data is insufficient for a magnetic structure refinement, however it is apparent that the (010) Bragg peak at the lowest Q has the largest magnetic intensity and peaks at higher Q are much weaker.

F. Neutron single crystal quasi-Laue diffraction

An accurate determination of the magnetic structure of $NiPS_3$ from refinement of neutron powder diffraction is extremely difficult due to the, possibly insurmountable, problems of preferred orientation and sample amorphization. Consequently, neutron single crystal diffraction experiments were attempted.

The VIVALDI diffractometer at the Institut Laue-Langevin [26] was used to collect quasi-Laue neutron scattering patterns. The instrument has a cylindrical image-plate detector with a vertical axis and an incident neutron beam wavelength band

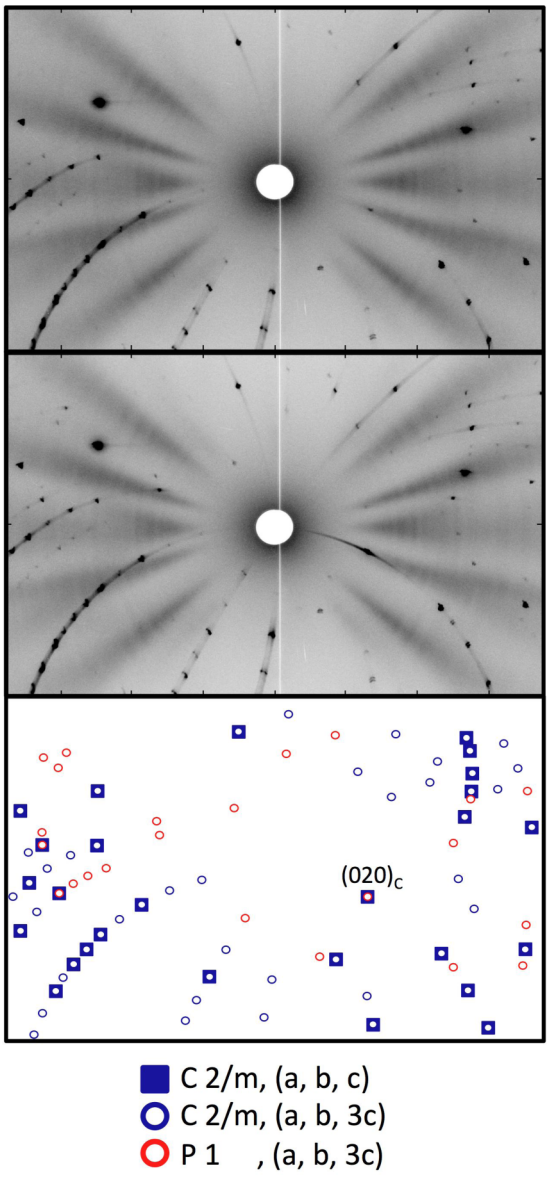

FIG. 8. (Color online) Laue diffraction measurements of $NiPS_3$ at 300 K (top panel) and 2 K (middle panel), along with the calculated positions of the Laue spots for different unit cell sizes and space groups (bottom panel). The peaks at 300 K are purely nuclear and could all be indexed using a $C2/m$ space group only if the c axis parameter listed in Table II was trebled. The Laue spot labeled $(020)_C$ can be indexed using both sets of lattice parameters. Extra peaks are visible in the 2 K data, and these could be indexed if the C centering was removed.

width of 0.8 to 5.2 Å. The crystal was carefully wrapped in a small amount of aluminum foil and was then glued to a pin, guaranteeing that the glue did not come into contact with the crystal. The crystal was placed in the detector on the cylindrical axis, and the temperature was controlled between 300 and 2 K with a helium cryostat. Measurements were made at selected fixed positions of the sample rotation about the vertical axis.

Figure 8 shows typical Laue patterns at 300 and 2 K. The sample orientation is the same for both measurements. The Laue spots are irregular in shape and show substantial structure. Furthermore, large streaks of intensity are visible

in some reciprocal lattice planes. Once the Laue patterns were indexed, the streaks were shown to be parallel to the c^* axis. The patterns are representative of the two-dimensional nature of the structure, which is prone to stacking faults of the ab planes. The presence of the streaks is not inconsistent with the powder data as the intensities in the streaks are very small in comparison to those of the Bragg peaks. Any asymmetry in the powder line shapes due to the streaks will be lost in the background. The streaks have been examined in detail with x-ray single crystal diffraction [27] and have been seen in neutron Laue diffraction data from a sister compound, $FePS_3$ [8].

High quality Laue data can be analyzed to determine the crystal structure. Unfortunately, the quality of the data from the $NiPS_3$ crystal was insufficient for a rigorous treatment of the data. The structure and smearing of the Laue spots meant that the intensities in the individual spots, necessary for a structure refinement, could not be reliably determined. The Laue data were therefore not used to refine the full magnetic structure. The Laue spots could, however, be indexed.

The orientation of the crystal was refined from the images using the CCP4 software suite [28,29] and, while the Laue spots are not δ functions, the crystal was found to be untwinned. Many, but not all, of the Laue spots could be indexed using the $C2/m$ space group and the lattice parameters from the literature [17]. All of the spots at all orientations could be indexed if the c-axis parameter was tripled. A tripling of the c axis is not unexpected. The monoclinic structure of the MPS_3 compounds is only slightly distorted from being hexagonal with trigonal symmetry, with a periodicity of three unit cells along c. Similar peaks have been observed and explained in x-ray powder diffraction [30] and single crystal diffraction [27] experiments. Small distortions and short-ranged order will give rise to Bragg-like features at the $l = 1/3$ positions.

Cooling to 2 K resulted in the appearance of a large number of new Laue spots. These spots could be indexed by removing the C centering from the space group, effectively indexing the pattern with using $P1$. This is a natural result of introducing a [010] propagation vector. There appear to be no spots at incommensurate positions. The indexed positions are all marked in the lowest panel of Fig. 8, along with the convention used for indexing.

The magnetic spots in the pattern are generally quite weak, with one notable exception marked as $(020)_C$ in the lowest panel of Fig. 8. This spot is present, but weak, at 300 K. At 2 K the spot is considerably stronger. This position could be indexed using all three conventions. It indexes as (020) if C centering is used, or (010) if C centering is removed. The intensity at high temperature is due to the (020) nuclear Bragg peak. The low-temperature change marks the emergence of the (010) magnetic peak observed by powder diffraction. Its intensity is superimposed on the (020) nuclear Bragg peak, which appears at the same position in Laue diffraction. The spot also shows prominent extension along the [00l] direction at 2 K, which indicates that the magnetic structure also has a two-dimensional nature.

G. Neutron single crystal monochromatic diffraction

The Laue patterns provided a reciprocal space map for the sample, identifying the likely space group and proving that there was no incommensurate order. This experiment also showed that there are indeed a large number of magnetic Bragg peaks that can be measured in a single-crystal neutron diffraction experiment. Thus, the sample was subsequently taken to monochromatic single crystal diffractometers at the ILL to refine the magnetic structure. Although data collection is slower, monochromatic diffractometers have the great advantage that the wavelength and incident intensity are well known, and it is easier to establish accurately the integrated intensities of irregular peak shapes. The two instruments used were D10, with a wavelength of $\lambda = 2.36$ Å, and D23, with a wavelength of $\lambda = 1.173$ Å.

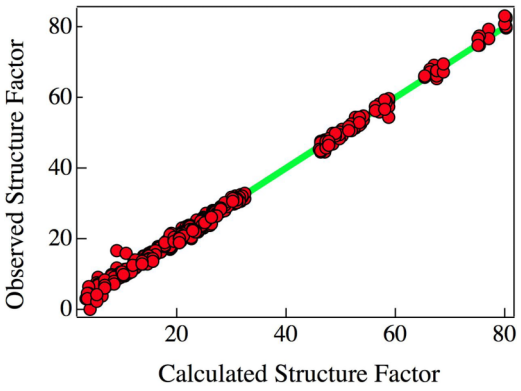

FIG. 9. (Color online) Observed versus calculated nuclear structure factors from refining the nuclear structure of $NiPS_3$ at 2 K. The peaks were indexed with the $C2/m$ space group.

The nuclear Bragg peak intensities were collected and the structure was refined using the FULLPROF program [19], starting with the parameters determined from x-ray diffraction by Ouvrard *et al.* [7]. The mixing of site occupancies for the Ni and the P was again permitted and its inclusion resulted in a substantial improvement to the structural refinement. The x and z positions for the P $4i$ and $8j$ positions were again constrained to be equivalent to be consistent with the x-ray powder diffraction measurements as removing the constraint resulted in only an incremental change to the quality of the refinement. The measured structure corresponded to that detailed in the literature. Figure 9 shows the comparison between the calculated and observed structure factors for the sample. The lattice parameters and site occupancies are listed in Table III, and they are quite close to the values in the literature. The Ni and P stoichiometries were allowed to vary independently in the fits, with the best fit giving a final global composition of $Ni_{0.984}P_{0.984}S_3$.

The values for the site disorder are coherent with those given in Table II. The values appear to be relatively large, however some caution must be applied. Stacking faults are clearly present in the crystal, as evident from the extended streaks in Fig. 8. The subsequent analysis might therefore be prone to some systematic errors. These errors are unlikely to affect the magnetic symmetries, but might affect the moment orientations, particularly on the minority Ni $2a$ sites.

Measurements at $l = 1/3$ positions identified weak Bragg-like features consistent with the observations in the neutron Laue diffraction measurements. The crystal structure of $NiPS_3$ is only slightly removed from being hexagonal, and the $l = 1/3$ features are consistent with the crystal having some small

TABLE III. Refined atomic coordinates for $NiPS_3$ at 2 K from monochromatic neutron single crystal diffraction in the space group $C2/m$. The refined lattice parameters were $a = 5.811(4)$, $b = 10.064(3)$, $c = 6.594(5)$ Å, and $\beta = 106.997(6)^\circ$ and the residuals were ${}_wR_{f2} = 6.30\%$ and $\chi^2 = 12.48$. The definition for the occupancies is consistent with Table II. The ratio of Ni in the $4g : 2a$ sites was 88 : 12 and the ratio of P occupying the $4i : 8j$ sites was 76.6 : 23.4.

Atom	Wyckoff position	x	y	z	B_{iso}	Occupancy
Ni(1)	$4g$	0	0.33335(6)	0	0.10(2)	0.866(36)
P(1)	$4i$	0.0588(2)	0	0.1700(3)	0.10(4)	0.754(48)
S(1)	$4i$	0.7427(3)	0	0.2442(5)	0.30(4)	1
S(2)	$8j$	0.2508(2)	0.1693(1)	0.2433(3)	0.27(3)	1
Ni(2)	$2a$	0	0	0	0.7(1)	0.236(4)
P(2)	$8j$	0.0588(2)	0.3335(7)	0.1700(3)	0.2(2)	0.115(5)

hexagonal distortion [30]. The distortion was not expected to have a large impact on the subsequent analysis, although a detailed examination of the distortion and its possible influence on the magnetism may be the subject of a future study.

Group theory and representation analysis were used to determine the irreducible representations compatible with the magnetic structure using a propagation vector of [010] via the BasIreps program within the FULLPROF suite. Four possible irreducible representations, whose symmetry operators are listed in Table IV, were found and they were tested while refining the magnetic Bragg peaks at 2 K using the scaling and Debye-Waller factors determined from the nuclear structure refinement. The majority of the Ni atoms are located at the four Ni $4g$ sites in the unit cell. The only representation that gives an adequate match to the magnetic Bragg peak intensities for these sites is IRep(4). There are two Ni $2a$ positions in the unit cell, and these have a minority occupancy. The best fits to the data showed that the symmetry for these sites are given by a combination of IRep(1) and IRep(3).

A refinement of the collected integrated intensities was then performed. The resulting moment orientations are shown in Table V. The comparison between the calculated and measured magnetic structure factors, shown in Fig. 10, demonstrates that the model is not ideal. It is highly likely that the discrepancies are due to the two-dimensional nature of the sample, both in its magnetic structure and due to stacking faults inducing disorder, causing many magnetic Bragg peaks to be extended along c^* and thus making it difficult to capture fully the integrated intensity of the peaks.

TABLE IV. The symmetry operators associated with the four possible irreducible representations of the magnetic structure, based on the application of a [010] propagation vector to the nuclear structure described in Table III.

Symmetry 1 1 : (0,0,0)	Symmetry 2 2 : (0, y, 0)	Symmetry 3 −1 : (0,0,0)	Symmetry 4 m : (x,0,z)	
IRep(1)	1	1	1	1
IRep(2)	1	1	−1	−1
IRep(3)	1	−1	1	−1
IRep(4)	1	−1	−1	1

TABLE V. The magnetic moment components refined at 2 K for the majority [site Ni(1)] and minority [site Ni(2)] Ni site positions in the unit cell. The Ni magnetic moment amplitudes are 1.05 and 1.06 μ_B for site 1 and site 2, respectively.

	Position			Moment		
	x	y	z	x	y	z
Site 1: Ni(1)	0	0.333	0	0.94(3)	0	−0.26(4)
Ni(2)	0	0.666	0	−0.94(3)	0	0.26(4)
Ni(3)	0.5	0.833	0	−0.94(3)	0	0.26(4)
Ni(4)	0.5	0.166	0	0.94(3)	0	−0.26(4)
Site 2: Ni(1)	0	0	0	1.0(5)	0.5(6)	0.0(9)
Ni(2)	0.5	0.5	0	−1.0(5)	−0.5(6)	−0.0(9)

It should be noted that the quality of the refinement when only the majority Ni $4g$ sites were included did not improve over the refinement when moments were allowed on both the $4g$ and $2a$ sites. Furthermore, the refined structure obtained for the majority Ni $4g$ sites was almost independent of the magnetic order refined for the minority $2a$ sites. The magnetic refinement of the Ni $4g$ sites appears to be robust, while far less confidence may be given to the moment directions found for the Ni $2a$ sites. For this reason, only the moment orientations for the majority $4g$ sites are shown in Fig. 10 while, for completeness, the refined orientations for both sites are shown in Table V. As already mentioned above, these Ni $2a$ sites are probably due to stacking faults. There might well be some disorder in the magnetism, although there is no direct proof of this in the measurements.

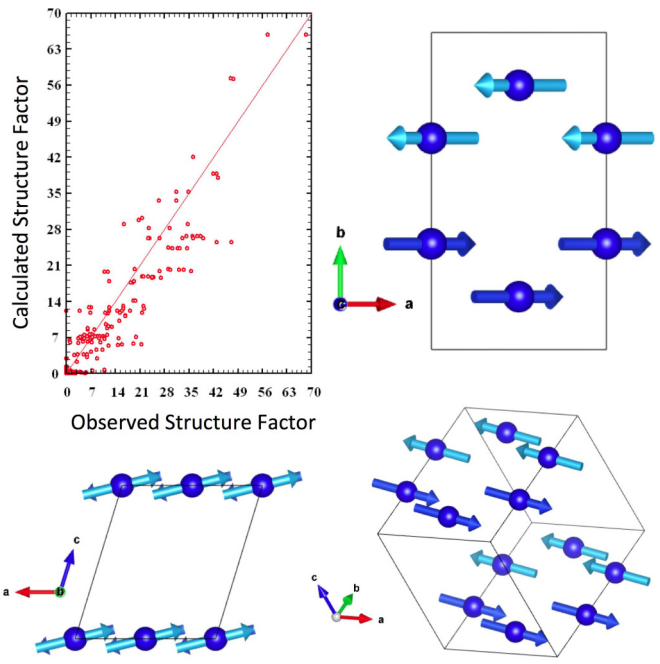

FIG. 10. (Color online) Observed versus calculated magnetic structure factors of $NiPS_3$ at 2 K using the best model yielding the refinement residuals of ${}_wR_{f2} = 23.8\%$ and $\chi^2 = 6.19$. The refined magnetic moment orientations are given in Table V. The proposed magnetic structure is also shown with various orientations, created using the VESTA program [13].

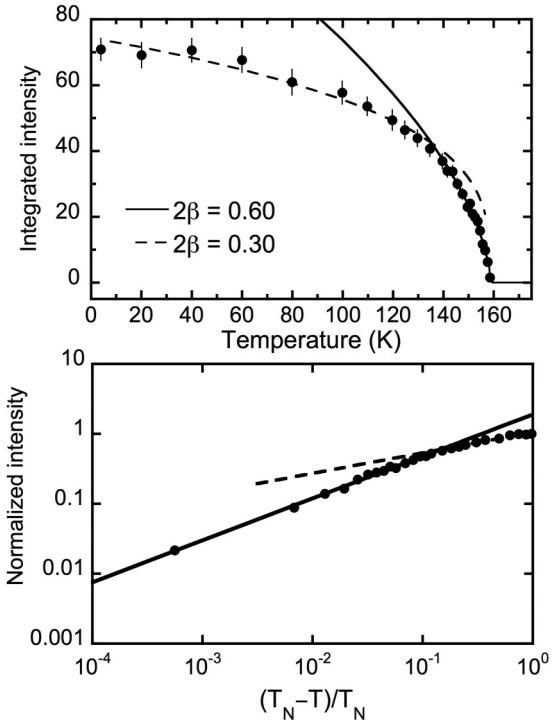

FIG. 11. Temperature dependence of the intensity of the (010) Bragg peak. Fitting a power law to the higher temperature data gives a Néel temperature of $T_N = 158.65(2)$ K and an exponent of $2\beta = 0.60 \pm 0.01$. Fitting the low temperature data when plotted against the reduced temperature relative to the fitted T_N gave an exponent of $2\beta = 0.30 \pm 0.01$. The upper panel shows the data and fits on a linear scale. The lower panel shows the same data and fits, normalized to the intensity at the lowest temperature and plotted against the reduced temperature.

The moment magnitudes were found to be 1.05 and 1.06 μ_B for the Ni(1) and Ni(2) sites, respectively. This is smaller than the expected $2\mu_B$ for the spin-only moment on a Ni^{2+} ion. The difference may be due to disorder and a reduction in the size of the ordered moment, although it is tantalizing to consider the the presence of quantum fluctuations which might not be negligible in a $S = 1$ system.

Nevertheless, the derived magnetic structure corresponds far better to the magnetic susceptibility data presented here and previously [3]. The moments on the Ni(1) positions are pointing mostly along the a direction with a small component along c, thus explaining why the smallest low-temperature susceptibility in Fig. 4 is along a, and is also nonzero.

The integrated intensity of the (010) magnetic Bragg peak was followed as a function of temperature. The intensity of the peak is proportional to the sublattice magnetization squared. The data are shown in Fig. 11. The intensities are roughly constant up to ~40 K. They then fall monotonically with increasing temperature until the Néel temperature, indicating that $NiPS_3$ undergoes a critical phase transition.

The data were correspondingly fitted with a power law to determine T_N, and to determine the critical exponent for the magnetization β. Attempts to fit the entire data range with a unique value for β were unsatisfactory. Hence, only the data just below T_N were initially fitted, giving $T_N =$ 158.65(2) K. This value was subsequently used to calculate a reduced temperature scale $(T_N - T)/T_N$. The data were then normalized to the intensity at the lowest temperature, and a plot showing the normalized data plotted on a log-log scale against the reduced temperature is shown in the lower panel of Fig. 11. The data appear to show a crossover in the critical behavior at $T \sim 0.9T_N$. The data above and below this point were independently fitted. The resulting exponent for $T < 0.9T_N$ was $2\beta = 0.30 \pm 0.01$. The exponent doubled to be $2\beta = 0.60 \pm 0.01$ close to T_N.

III. DISCUSSION

The data presented in the preceding sections show many discrepancies when compared to those in previous publications. Many of the discrepancies appear to stem from the difficulties in preparing $NiPS_3$ samples for measurements. Powdered samples suffer from a high degree of preferred orientation. Furthermore, the substantial nuclear short-ranged order and nuclear-spin-incoherent scattering apparent in Fig. 7 suggest that the act of grinding the sample to create the powder may result in some amorphization. The latter effect, if true, is fortunately a minor consideration for the magnetic studies as amorphous and crystalline $NiPS_3$ appear to have distinct and easily separable magnetic properties [24]. Preferred orientation, however, severely compromises the determination of both nuclear (atomic) and magnetic structures using powder diffraction techniques. It is possible to index the Bragg peaks, and the data presented here agree with the previously published magnetic structure [2] that the magnetic propagation vector is $\mathbf{k} = [010]$, however it is far more difficult to determine the direction of the moments from powder diffraction measurements.

The investigation of the magnetic properties of these compounds is therefore much better performed using single crystals. Even so, a great deal of care needs to be taken in preparing the samples. The act of gluing a sample to a support can have a marked impact on the magnetic properties, showing anisotropic paramagnetic susceptibilities reminiscent of previously published data [3,9]. The data in Fig. 4 were measured on an as-prepared single crystal that was not glued. While the magnitudes of the susceptibility agree with previous studies [3,9], the results show an isotropic susceptibility above T_N.

Single-crystal neutron diffraction is the appropriate technique for determining a magnetic structure for $NiPS_3$, but even then the data must be interpreted with care. The two-dimensional nature of $NiPS_3$ creates rodlike scattering in reciprocal space. This is observed for the nuclear (atomic) structure [27] and the data in Fig. 8 shows that it is also true for the magnetic structure. It is difficult to guarantee that the full magnetic intensity for a Bragg peak has been measured to determine the moment orientations and the quality of the structure refinement, shown in Fig. 10, can at best be described as reasonable. Nevertheless, the magnetic structure shown in the figure is now acceptable, being consistent with the susceptibility data.

The critical exponents shown in Fig. 11 may be compared to those expected for various Hamiltonians and universality classes [31]. Taroni *et al.* have presented a comprehensive survey of the values for β for two-dimensional systems,

showing that they lie between $0.1 \leqslant \beta \leqslant 0.25$ [32]. The Ising and XY Hamiltonians in two dimensions are two important models that have magnetic ordering. The two-dimensional Ising model is exactly solvable, giving an exponent of $\beta = 0.125$ below the transition temperature [33]. The critical behavior for $FePS_3$ falls into this universality class [8]. The XY model displays an ordering temperature associated with the Kosterlitz-Thouless transition, and a value of $\beta = 0.231$ has been calculated below this temperature [34]. Despite being well described by a Heisenberg Hamiltonian, the critical behavior of $MnPS_3$ appears to correspond to this universality class [5].

The low-temperature value of $\beta = 0.15$ for $NiPS_3$ lies within the range given by Taroni *et al.*, which is consistent with its two-dimensional nature. The moment orientations in the ordered phase and the isotropic nature of the susceptibility above T_N suggest that the compound would be best described by some form of Heisenberg Hamiltonian with weak in-plane anisotropy. However, the low-temperature value for β for $NiPS_3$ does not correspond to either the Ising or XY values. The reason for this is not immediately apparent.

A value of $\beta > 0.3$ is characteristic of three-dimensional antiferromagnets [31]. The crossover to $\beta = 0.30$ close to T_N is consistent with the onset of three-dimensional correlations in XY-like materials [34]. A similar crossover was also observed in $MnPS_3$ [5].

The two-dimensional magnetic structure of $NiPS_3$, with ferromagnetic chains that are antiferromagnetically coupled, is sometimes referred to as the "zigzag" structure. The moments in $NiPS_3$ lie in the ab planes. Two other honeycomb systems have very similar structures and moment orientations to $NiPS_3$. These compounds are $BaNi_2(AsO_4)_2$ [35,36] and Na_2IrO_3 [10].

$BaNi_2(AsO_4)_2$ appears to be an example of two-dimensional XY antiferromagnet. It orders below $T_N \sim 19$ K, and its paramagnetic susceptibility is anisotropic. The spin-wave dispersion can be modeled with a simple Hamiltonian if exchange interactions up to the third-nearest neighbor are included, and spin-wave theory calculations show that the magnetic structure is stable [37,38]. The critical behavior is somewhat ambiguous. The critical exponent for the magnetization is $\beta \simeq 0.135$ which is close to that expected for the two-dimensional Ising model. The in-plane magnetic correlation is fitted almost equally well either using a power law, giving an exponent of $\nu = 1.0$ which is expected for the Ising model, or the Kosterlitz-Thouless expression expected for an XY model. Specific heat data suggests that the compound is more XY-like than Ising-like, however. Like $NiPS_3$, $BaNi_2(AsO_4)_2$ has a crossover to three-dimensional behavior with $\beta = 0.33$ close to T_N [35,36].

Na_2IrO_3 orders below $T_N = 15.3$ K. It is a candidate for the Kitaev-Heisenberg model due to anisotropic interactions induced by the strong spin-orbit coupling of the iridium, although the presence of exchange interactions beyond the first nearest neighbor appears to perturb ideal behavior. The magnitudes of these exchange interactions are yet to be quantified. There has been a great deal of theoretical interest in the compound, including the calculations of stability conditions and critical behavior [39–41]. It may be that calculations based on simpler Hamiltonians (cf. Refs. [37,38]) are also relevant.

It is thus of interest to measure the spin-wave dispersion of $NiPS_3$ to determine the exchange interactions which, based on the values determined for $MnPS_3$ [42] and $FePS_3$ [5], are likely to extend to the third-nearest neighbor. Measurements of the spin dynamics using neutron inelastic scattering are currently being performed.

IV. CONCLUSIONS

Our measurements show that accurate and reproducible measurements of the magnetic properties of $NiPS_3$ require single crystals, and these crystals must be carefully handled. $NiPS_3$ orders magnetically with a propagation vector of $\mathbf{k} = [010]$ with the moment direction found to be mostly along the a axis, which is in agreement with magnetic susceptibility measurements. The anisotropy appears to be smaller than previously considered, such that the susceptibility above T_N is isotropic. The sublattice magnetization scales as a power law of the reduced temperature, with a nonuniversal exponent representative of two-dimensional magnets for $T \lesssim 0.9T_N$ and with an exponent representative of three-dimensional order for $0.9T_N \lesssim T \leqslant T_N$. A study of the spin-wave dynamics is now required.

ACKNOWLEDGMENTS

The authors wish to thank the European Synchrotron Radiation Source, the Institut Laue-Langevin, and the Bragg Institute, ANSTO, for the use of their instruments. Equally, the authors thank E. Eyraud from Institut Néel for the technical support in the SQUID magnetometry measurements. A.R.W. performed part of this work while on sabbatical at Monash University, funded by a Monash University Research Grant, and would like to thank the university and T.J.H. for the financial support, and Professor Keith Murray in the Department of Chemistry for the use of his SQUID. Finally, we thank Dr. G. Nilsen and Dr. T. Ziman for stimulating discussions.

[1] V. Grasso and L. Silipigni, Riv. Nuovo Cimento **25**, 1 (2002).
[2] R. Brec, Solid State Ionics **22**, 3 (1986).
[3] P. A. Joy and S. Vasudevan, Phys. Rev. B **46**, 5425 (1992).
[4] E. Ressouche, M. Loire, V. Simonet, R. Ballou, A. Stunault, and A. Wildes, Phys. Rev. B **82**, 100408(R) (2010).
[5] A. R. Wildes, H. M. Rønnow, B. Roessli, M. J. Harris, and K. W. Godfrey, Phys. Rev. B **74**, 094422 (2006).
[6] A. R. Wildes, K. C. Rule, R. I. Bewley, M. Enderle, and T. J. Hicks, J. Phys.: Condens. Matter **24**, 416004 (2012).
[7] G. Ouvrard, R. Brec, and J. Rouxel, Mater. Res. Bull. **20**, 1181 (1985).
[8] K. C. Rule, G. J. McIntyre, S. J. Kennedy, and T. J. Hicks, Phys. Rev. B **76**, 134402 (2007).
[9] N. Chandrasekharan and S. Vasudevan, J. Phys.: Condens. Matter **6**, 4569 (1994).
[10] S. K. Choi, R. Coldea, A. N. Kilmogorov, T. Lancaster, I. I. Mazin, S. J. Blundell, P. G. Radaelli, Y. Singh, P. Gegenwart, K. R. Choi *et al.*, Phys. Rev. Lett. **108**, 127204 (2012).

[11] S. Rosenblum, A. H. Francis, and R. Merlin, Phys. Rev. B **49**, 4352 (1994).
[12] S. S. Rosenblum and R. Merlin, Phys. Rev. B **59**, 6317 (1999).
[13] K. Momma and F. Izumi, J. Appl. Crystallogr. **44**, 1272 (2011).
[14] See Supplemental Material at http://link.aps.org/supplemental/10.1103/PhysRevB.92.224408 for magnetization measurements on a glued crystal, for medium resolution neutron powder diffraction data, and for neutron diffraction with polarization analysis measured at 300 K.
[15] H. M. Rietveld, J. Appl. Crystallogr. **2**, 65 (1969).
[16] A. Larson and R. V. Dreele, General Structure Analysis System (GSAS), Los Alamos National Laboratory Report LAUR 86-748 (1994).
[17] G. Ouvrard, R. Brec, and J. Rouxel, C. R. Acad. Sci. Paris Série II **294**, 971 (1982).
[18] D. A. Cruse and M. Gerloch, J. Chem. Soc. Dalton Trans. **1977**, 152 (1977).
[19] J. Rodriguez-Carvajal, Physica B **192**, 55 (1993).
[20] J. R. Stewart, P. Deen, K. H. Andersen, H. Schober, J.-F. Barthélémy, J. M. Hillier, A. P. Murani, T. Hayes, and B. Lindenau, J. Appl. Crystallogr. **42**, 69 (2009).
[21] O. Schärpf and H. Capellmann, Phys. Status Solidi A **135**, 359 (1993).
[22] P. J. Brown, in *International Tables for Crystallography*, edited by A. J. C. Wilson (Kluwer, Dordrecht, 1995), Vol. C, p. 391.
[23] V. F. Sears, Neutron News **3**(3), 26 (1992).
[24] E. Prouzet, G. Ouvrard, R. Brec, and P. Segineau, Solid State Ionics **31**, 79 (1988).
[25] P. Fragnaud, E. Prouzet, G. Ouvrard, J. L. Mansot, C. Payen, R. Brec, and H. Dexpert, J. Non-Cryst. Solids **160**, 1 (1993).
[26] G. J. McIntyre, M.-H. Lemée-Cailleau, and C. Wilkinson, Physica B **385-386**, 1055 (2006).
[27] D. J. Goossens, D. James, J. Dong, R. E. Whitfield, L. Norén, and R. L. Withers, J. Phys.: Condens. Matter **23**, 065401 (2011).
[28] J. W. Campbell, J. Appl. Crystallogr. **28**, 228 (1995).
[29] J. Helliwell, J. Habash, D. Cruickshank, M. Harding, T. Greenhough, J. Campbell, I. Clifton, M. Elder, P. Machin, M. Papiz *et al.*, J. Appl. Crystallogr. **22**, 483 (1989).
[30] G. Ouvrard and R. Brec, Eur. J. Solid State Inorg. Chem. **27**, 477 (1990).
[31] A. Pelissetto and E. Vicari, Phys. Rep. **368**, 549 (2002).
[32] A. Taroni, S. T. Bramwell, and P. C. W. Holdsworth, J. Phys.: Condens. Matter **20**, 275233 (2008).
[33] L. Onsager, Phys. Rev. **65**, 117 (1944).
[34] S. T. Bramwell and P. C. W. Holdsworth, J. Phys.: Condens. Matter **5**, L53 (1993).
[35] L. P. Regnault, J. Y. Henry, J. Rossat-Mignod, and A. de Combarieu, J. Magn. Magn. Mater. **15-18**, 1021 (1980).
[36] L. P. Regnault and J. Rossat-Mignod, in *Magnetic Properties of Layered Transition Metal Compounds*, edited by L. J. de Jongh (Kluwer Academic, Dordrecht, the Netherlands, 1990).
[37] E. Rastelli, A. Tassi, and L. Reatto, Physica B **97**, 1 (1979).
[38] J. B. Fouet, P. Sindzingre, and C. Lhuillier, Eur. Phys. J. B **20**, 241 (2001).
[39] J. Chaloupka, G. Jackeli, and G. Khaliullin, Phys. Rev. Lett. **110**, 097204 (2013).
[40] Y. Sizyuk, C. Price, P. Wölfle, and N. B. Perkins, Phys. Rev. B **90**, 155126 (2014).
[41] C. C. Price and N. B. Perkins, Phys. Rev. Lett. **109**, 187201 (2012).
[42] A. R. Wildes, B. Roessli, B. Lebech, and K. W. Godfrey, J. Phys.: Condens. Matter **10**, 6417 (1998).